Influences Of Process Parameters On Twin Tungsten Electrode - Wire Electrode Indirect Arc Additive Manufacturing Process

Yanli Zhu[1*], Hong He[2], Dianguo Ma[1], Haibo Liu[1], Peimin Li[1], and Lincai Zhang[1*]

[1] *School of Mechanical and Electrical Engineering, Zaozhuang University, Zaozhuang, 277160, China*
[2] *Tengzhou Wanbao Stroller Co., Ltd., Tengzhou, 277500, China*
[*] *Corresponding author. E-mail: zhuyanli007@163.com (Y. Zhu); vicande@hotmail.com (L. Zhang)*

Received: Mar. 04, 2026; Accepted: Apr. 21, 2026

In this paper, the effects of wire-tungsten (d_1) and tungsten-tungsten (d_2) spacing on the forming characteristic of twin tungsten electrode - wire electrode indirect arc (TTWIA) additive manufacturing were comprehensively studied. The arc shape, droplet transfer, and molten pool behavior were recorded respectively. Results showed that as d_1 or d_2 increased, the arc shape of TTWIA diverged and the coupling intensity was weakened. Besides, the liquid stream became thick as well as the larger droplet diameter and lower transfer frequency, mainly attributed to the reduced arc current density and detachment forces acting on the droplet. Additionally, on account of the decreased arc pressure and droplet impingement force on the molten pool, the transverse flow tendency of liquid metal was diminished, and the molten pool width of TTWIA decreased, which was adverse to the spreading of the deposited layer. Moreover, the forming quality of the thin-walled part deteriorated, together with the increased surface roughness and reduced material utilization rate, which mainly attributed to the instability of the molten pool because of the lowered normal reaction acting on the molten pool of the present deposited layer.

Keywords: TTWIA; Wire and arc additive manufacturing; Forming characteristic; Process parameter; Arc shape

http://dx.doi.org/10.6180/jase.202609_32.040

1. Introduction

Wire and arc additive manufacturing (WAAM) offered advantages such as high material utilization, fast forming speed, and low manufacturing cost, making it particularly suitable for the rapid near-net shaping of large, complex structural components [1, 2]. Tungsten inert gas (TIG) was a typical arc heat source applied to WAAM, because of high process stability and fabricating components with a wide variety of metal materials [3, 4]. However, the deposition efficiency in TIG process was only $1-2$ kg/h, which was difficult to satisfy the great demand for high productivity in modern manufacturing industry [5]. In double-wire TIG additive manufacturing [6], a 50% increase in deposition efficiency and a 16.14% increase in tensile strength for the component compared with single-wire TIG process. Moreover, the deposition rate during hotwire TIG process was approximately twice that during cold-wire TIG [7]. Nevertheless, the lowresistance material could not be preheated, and the magnetic blow also occurred during hot-wire TIG process. To solve the above problems, an assistant arc [8] and an induction heating system [9] were separately brought in hot-wire TIG process. Additionally, in twin-electrode TIG additive manufacturing [10], a 2.7 kg/h wire deposition rate was achieved, which was nearly twice that in conventional TIG.

Although the above advanced methods could enhance the deposition efficiency to some extent, the wire still primarily relied on absorbing heat from the molten pool to complete melting. In other words, the arc energy and wire deposition rate still remained coupled. In WAAM process, excessive arc energy intensified heat accumulation during

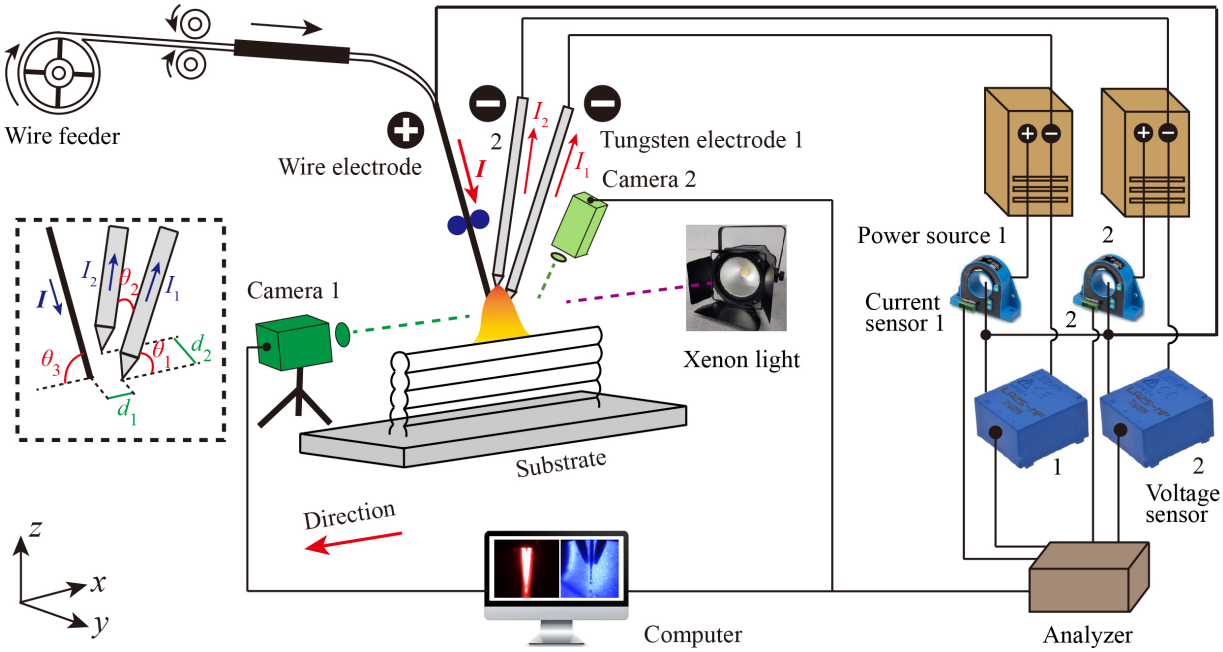

Fig. 1. Schematic diagram of TTWIA additive manufacturing and signal and image acquisition system.

deposition, resulting in various defects, namely high residual stress [11], layer collapse [12], cracking [13], porosity [14], and coarse grain structure [15], which severely compromised the geometric accuracy and forming quality of the components. In recent years, to address the severe heat accumulation issue in WAAM process, researchers had proposed several control strategies, namely adjusting process parameters [16, 17] or introducing external auxiliary cooling [18, 19]. However, these methods inevitably compromised the forming efficiency and limited the allowable deposition size. Therefore, developing advanced arc heat source with low thermal input represented an effective solution to mitigate severe heat accumulation during WAAM process.

Unlike conventional TIG arc, the arcing-wire TIG [20, 21] process not only maintained the main arc, but also established a secondary arc between the tungsten electrode and the filler wire, which could achieve a reasonable allocation between the melting heat of welding wire and workpiece heat input. Besides, in single tungsten electrode - wire electrode indirect arc (STWIA) process, the tungsten electrode and filler wire were respectively linked to the negative and positive poles of the power supply, while the workpiece was not linked to the circuit [22]. Notably, the wire deposition rate of STWIA could reach 3.8 kg/h, which was approximately equal to that of gas metal arc (GMA). Notably, the heat input to the workpiece was extremely low, along with a low dilution rate. However, the components fabricated by STWIA additive manufacturing exhibited relatively weak surface quality and dimensional accuracy, mainly because of the poor wettability of the deposited layer.

The authors proposed a twin tungsten electrode - wire electrode indirect arc (TTWIA) [23, 24], in which the larger distribution radius of the heat source could optimize the magnitude and distribution of the arc force acting on molten pool and the energy transmitted to it, thereby obtaining a more stable molten pool compared with that of STWIA. Besides, the weld spreadability of TTWIA could be enhanced by applying an alternating parallel magnetic field [25]. Especially, the wetting angle of the single bead could decrease 31.5% and the layer width could increase 20.2% when the external excitation current was 39 A. Additionally, the authors preliminarily investigated the forming characteristics of multi-layer single-bead additive manufacturing by TTWIA [26], and found that arc current had a significant influence on molten pool behavior and forming accuracy. In this study, the images and signals during TTWIA additive manufacturing process were acquired by corresponding collection equipment, and the influence mechanisms of process parameters on the geometric accuracy of the components were analyzed in depth.

2. Experiment method

Fig. 1 illustrates the experimental setup of TTWIA additive manufacturing system consisting of two TIG power

sources and an auxiliary wire feeder. The two tungsten electrodes were separately linked to the negative poles of both power supplies, and the wire electrode was simultaneously linked to the positive poles of both power supplies, while the substrate was not linked to the circuit. The current in the wire electrode was equal to the sum of the currents in both tungsten electrodes ($I = I_1 + I_2$). A Q235 steel plate with dimensions of 200 mm × 150 mm × 10 mm was employed as the substrate, and a ∅1.2 mm welding wire (ER50-6) applied was also carbon steel. During deposition, the welding torches remained stationary, white the substrate moved along x direction, in a deposited direction of wire electrode in front and tungsten electrodes in back. Thin-walled component was formed using the same-direction stacking method layer by layer, with a 60 s interval between adjacent layers. The specific deposition conditions in TTWIA additive manufacturing are listed in Table 1. Besides, the electrode position parameters of TTWIA and other experimental parameters were same as reference [26].

The arc morphology and droplet transfer process of TTWIA were collected by a camera 1. Notably, to better observe the arc behavior of TTWIA, the arc was made burn in the air rather than on the substrate. Besides, a xenon lamp was employed as the backlight when collecting the droplet behavior to remove the arc light disturbance. Additionally, a camera 2 was employed to collect the molten pool behavior of TTWIA. It should be noted that the pixel resolution, exposure time, and acquisition frequency of both cameras were set to 320 × 240 pixel, 500μ s, and 2000 fps separately. Two voltage sensors were used to measure the output voltages of the two power supplies, and two current sensors were used for the output currents, respectively. Finally, the electrical signals were processed and saved using a professional analyzer [27]. Metallographic specimens were wire-cut from the as-built thin-walled component along the direction perpendicular to the deposited bead. The specimens were corroded by a mixture of 4vol% nitric acid and 96vol% absolute alcohol for nearly 15 s , and then a scanner was employed to capture the macroscopic morphology of the specimen.

3. Results and discussion

3.1. Arc shape and droplet transfer

The typical arc shapes of TTWIA with different wire-tungsten (d_1) and tungsten-tungsten (d_2) distances are shown in Fig. 2. It could be seen that electrode spacing had a significant effect on arc shape of TTWIA. When both d_1 and d_2 were 2 mm (Fig. 2(a,e)), the arc shape was concentrated, with high straightness and coupling degree. As d_1 increased (Fig. 2(b,c)), the arc shape diverged and the arc width obviously increased. Besides, the arc gradually deflected toward the tungsten electrode sides. Likewise, as d_2 increased (Fig. 2(f,g)), the arc shape exhibited a similar variation trend. Especially when d_2 reached 5 mm (Fig. 2(h)), the arc presented excessive divergence, as well as weak coupling intensity and apparent fluctuation.

Fig. 2(d,i) show analysis of the forces on the arc of TTWIA. The arc conductive channel elongated and thus the arc current density decreased when d_1 increased, resulting in a slower wire melting rate. Consequently, the equilibrium position of the wire tip shifted toward the lower-left side of the tungsten electrode tip. Therefore, the resultant force direction of both the electromagnetic force (F_e) and plasma flow force (F_p) acting on the charged particles pointed toward the tungsten electrode sides. Similarly, when d_2 was relatively larger, the arc conductive channel became more elongated, resulting in a lower arc current density and weaker self-induced magnetic field strength. Consequently, the electromagnetic force F_{ed} acting on charged particles became relatively lower, which adversely affected the arc coupling interaction of TTWIA.

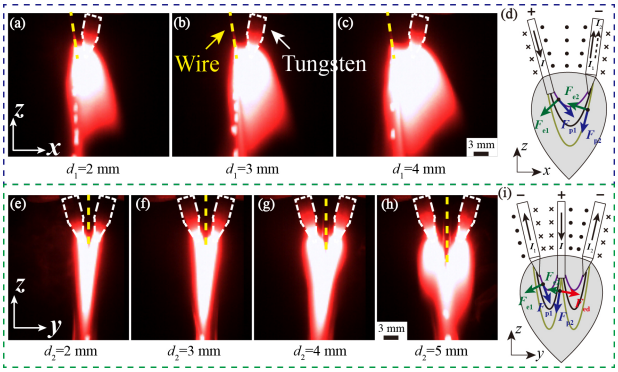

Fig. 2. Arc morphology of TTWIA under different wire-tungsten (d_1) and tungsten-tungsten (d_2) distances. (a) $d_1 = 2$ mm; (b) $d_1 = 3$ mm; (c) $d_1 = 4$ mm; (e) $d_2 = 2$ mm; (f) $d_2 = 3$ mm; (g) $d_2 = 4$ mm; (h) $d_2 = 5$ mm; (d, i) Acting forces on arc.

Fig. 3 shows typical droplet transfer behavior of TTWIA under different wire-tungsten (d_1) and tungsten-tungsten (d_2) distances. It could be seen that under different d_1 and d_2, necking phenomena occurred at the wire tip, and the diameter of the liquid stream was smaller than that of the wire. Therefore, the droplet transfer mode of TTWIA could be identified as streaming spray transfer in this experimental condition. When both d_1 and d_2 were 2 mm (Fig. 3(a,e)), the liquid stream presented a thin diameter, with a droplet diameter as small as 0.51 mm , while the droplet trans-

Table 1. Deposition condition.

No.	Arc current (A)	Wire feeding speed (m/min)	Travel speed (mm/s)	d_1 (mm)	d_2 (mm)
1	100 + 100	6.75	5	2	2
2	100 + 100	6.75	5	3	2
3	100 + 100	6.75	5	4	2
4	100 + 100	6.75	5	5	2
5	100 + 100	6.75	5	2	3
6	100 + 100	6.75	5	2	4
7	100 + 100	6.75	5	2	5

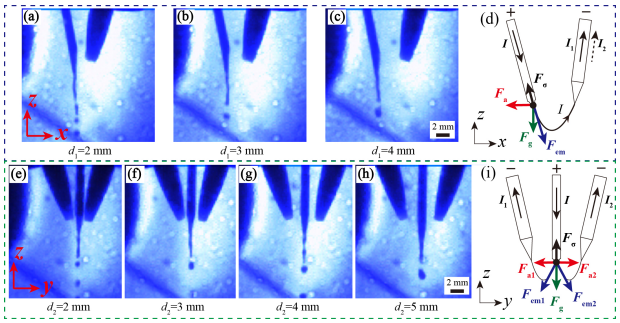

Fig. 3. Droplet transfer behaviors of TTWIA under different wire-tungsten (d_1) and tungsten-tungsten (d_2) distances. (a) $d_1 = 2$ mm; (b) $d_1 = 3$ mm; (c) $d_1 = 4$ mm; (e) $d_2 = 2$ mm; (f) $d_2 = 3$ mm; (g) $d_2 = 4$ mm; (h) $d_2 = 5$ mm; (d, i) Force analysis on droplet.

fer frequency reached up to 625 Hz . As the increase of d_1, the liquid stream became thicker, the droplet diameter increased, while the transfer frequency decreased, which indicated that the increasing d_1 was adverse to the smooth transfer process of the droplet. Likewise, as d_2 increased (Fig. 3(f, g)), the necking position on the wire tip continuously moved downward, while the droplet diameter gradually increased and the transfer frequency gradually decreased. Especially when d_2 increased to 5 mm (Fig. 3(h)), the vertical distance between the wire tip and the tungsten electrode tip further increased. In other words, the location where necking occurred at the end of the wire was farther away from the end of the tungsten electrode. Additionally, the diameter of the liquid stream was also thicker, with a droplet diameter of 0.76 mm and a transfer frequency of merely 268 Hz .

Fig. 3(d,i) show acting forces on the liquid droplet of TTWIA. The wire melting rate decreased owing to the reduced arc temperature caused by the increased d_1, which was prone to accumulate into a thicker liquid stream. Moreover, the heat absorbed by the droplet from the arc decreased, resulting in an increase in the surface tension F_σ acting on the droplet, and thus the resistance of the droplet detachment was enhanced. Additionally, the decrease in arc current density due to the increased d_1 reduced the electromagnetic force F_{em} and arc pressure F_{a} acting on the droplet, which suggested that the driving force for droplet detachment was decreased. Therefore, as d_1 increased, the droplet detachment process became difficult, with longer transfer period and larger droplet diameter. Likewise, the arc expanded due to the increased d_2, leading to a decrease in both arc current density and arc temperature. On the one hand, the wire melting rate decreased, which caused the tip position of the wire moved downward and further away from the tungsten electrode tip. On the other hand, the driving force of the droplet detachment decreased, primarily including the electromagnetic force F_{em} and arc pressure F_{a} , while the resistance of droplet detachment increased, namely the surface tension F_σ, which was unfavorable for the process of the smooth transfer of the droplet.

When the external of the power supply was a constant current characteristic, the voltage variation coefficient [23] could be used to evaluate the process stability according to statistical theory. The arc voltages and its variation coefficients of TTWIA under different wire-tungsten (d_1) and tungsten-tungsten (d_2) distances are shown in Fig. 4.

It was evident that as d_1 increased from 2 mm to 4 mm , the arc voltage of TTWIA progressively rose from 16.2 V to 19.8 V (Fig. 4(a)). The increase in d_1 led to an increase in arc width and arc energy dissipation, which caused the electric field strength of the arc increased based on the minimum voltage fundamental of the arc [28, 29]. Additionally, the arc voltage variation coefficient also increased as d_1 increased, indicating that a larger d_1 was adverse to the process stability. It was closely related to the decrease in the arc stiffness and the wire melting rate resulting from a larger d_1. Similarly, as d_2 increased from 2 mm to 4 mm (Fig. 4(b)), the arc voltage of TTWIA progressively rose increased from 16.2 V to 17.6 V . The increase in d_2 caused the arc expansion, and thus the heat dissipation from the arc to the surrounding environment increased, which consequently resulted in an elevation of the arc electric field intensity. Moreover, the variation coefficient of the arc voltage also exhibited a rise trend with the increase of d_2.

Notably, when d_2 reached 5 mm (Fig. 4(b)), a significant rise in this coefficient was observed. This suggested that the increment of d_2 would degrade the process stability, primarily because of the weaker coupling degree of the arc and lower wire melting speed at larger d_2.

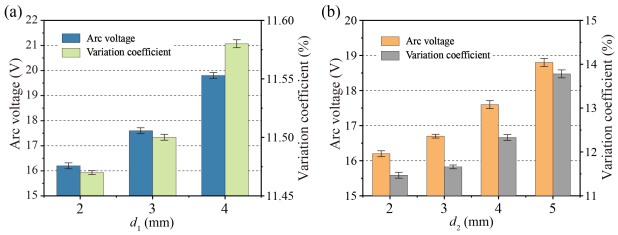

Fig. 4. Electrical parameters of TTWIA. (a) With different wire-tungsten (d_1) distances; (b) With different tungsten-tungsten (d_2) distances.

3.2. Molten pool behavior

The molten pool behavior of TTWIA with different wire-tungsten (d_1) and tungsten-tungsten (d_2) distances are shown in Fig. 5. When both d_1 and d_2 were 2 mm (Fig. 5(a)), the liquid metal achieved sufficient transverse spreading, resulting in a molten pool width of 7.24 mm . The transverse flow tendency of the liquid metal was diminished, and the molten pool width decreased as the increase of d_1 (Fig. 5(b)). However, when d_1 further increased to 4 mm , the liquid metal began to overflow from the deposition channel (Fig. 5(c)). Furthermore, when d_1 reached 5 mm (Fig. 5(d)), the stability of the molten pool deteriorated with apparent distortion, which was closely associated with the unstable arc behavior and droplet transfer process induced by the excessive d_1.

Likewise, the molten pool behavior of TTWIA presented a comparable variation pattern as the increase of d_2 (Fig. 5(e)). However, a pronounced oscillation emerged in the molten pool, and a surface depression was induced when d_2 reached 4 mm (Fig. 5(f)). Moreover, the stability of the molten pool further deteriorated with stronger oscillation and larger surface depression at a d_2 of 5 mm (Fig. 5(g)). This phenomenon mainly resulted from the significant instability of the arc shape and droplet transfer process induced by the excessive d_2.

Fig. 5(i,j) show the acting forces and convection pattern of the liquid metal. In the front, the molten pool was made flow outward and backward mainly by the action of arc pressure F_P and droplet impingement force F_D [30]. In the tail, the Marangoni force F_M drove the molten pool to flow from the boundary to the center of the molten pool [31].

As d_1 increased, F_P decreased because of the declined

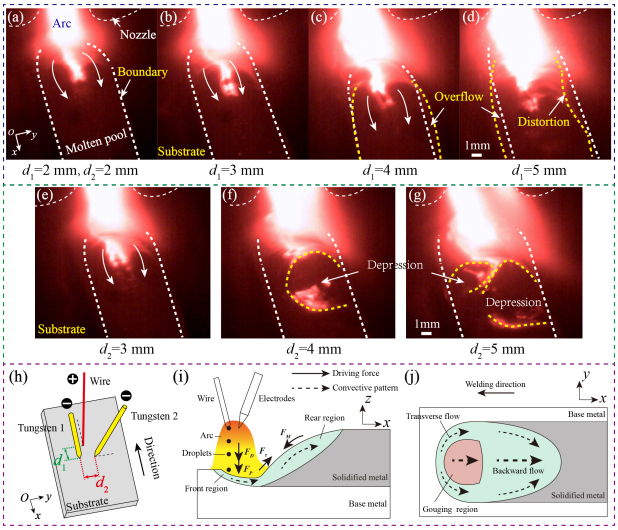

Fig. 5. Molten pool shapes of TTWIA. (a) $d_1 = 2$ mm, $d_2 = 2$ mm; (b) $d_1 = 3$ mm; (c) $d_1 = 4$ mm; (d) $d_1 = 5$ mm; (e) $d_2 = 3$ mm; (f) $d_2 = 4$ mm; (g) $d_2 = 5$ mm; (h) Schematic diagram of deposition process; (i,j) Acting forces and convection pattern of liquid metal.

arc current density, and F_D also decreased because of the reduced droplet transfer frequency, which suggested that the increase of d_1 minimized the driving force of the transverse convection of the liquid metal. Moreover, the increase in d_1 meant that the arc was elongated along the deposition direction, and thus the temperature distribution gradient of the molten pool decreased along the deposition direction. Therefore, F_M decreased and the suppression effect on the backward flow of the liquid metal was minimized, which was adverse to the transverse flow of the molten pool. Similarly, the driving force and the convection pattern of the molten pool presented variation trend as the increase of d_2.

3.3. Single-layer single-bead deposition process

Fig. 6 shows the appearances, cross sections, and geometric dimensions of the single beads by TTWIA with different wire-tungsten (d_1) and tungsten-tungsten (d_2) distances. When d_1 and d_2 were both 2 mm (Fig. 6(a,b)), the single bead was uniformly and smoothly formed with no defect, and the height/width ratio and wetting angle of the deposited layer were 0.45 and 80.2° respectively, which mainly resulted from the sufficient transverse convection of the molten pool(Fig. 5(a)). As d_1 increased (Fig. 6(c-f)), although a continuous deposited bead could still be achieved, both the height/width ratio and the wetting angle increased, which meant that the spreading of the single bead deteriorated. This was primarily because the transverse flow of the liquid metal in molten pool was reduced

on the condition of the increased d_1 (Fig. 5(b,c)). Specifically, the height/width ratio and wetting angle of the single bead separately reached 0.60 and 100.4° as d_1 was 4 mm , with the appearance of the slight spattering. Moreover, when d_1 further increased to 5 mm (Fig. 6(g)), the deposited layer became uneven with the large spatters and evident porosity. This was closely related to the worse protection and intensified oscillation in the molten pool caused by the excessive d_1.

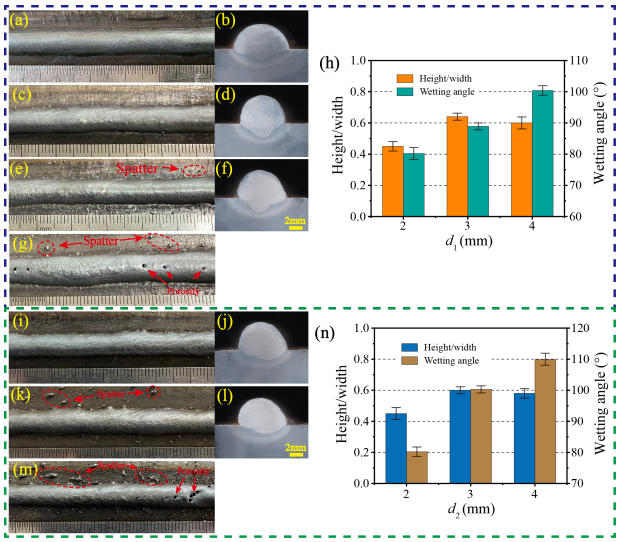

Fig. 6. Deposition formation and cross sections of TTWIA single-layer single-pass. (a,b) $d_1 = 2$ mm, $d_2 = 2$ mm; (c,d) $d_1 = 3$ mm; (e,f) $d_1 = 4$ mm; (g) $d_1 = 5$ mm; (h) Bead parameters with different d_1; (i,j) $d_2 = 3$ mm; (k,l) $d_2 = 4$ mm; (m) $d_2 = 5$ mm; (n) Bead parameters with different d_2.

Likewise, the spreading of the deposited bead decreased as d_2 increased, even if a smooth and continuous deposited bead could still be achieved, which was also mainly contributed by the diminished transverse convection of the molten pool in singled bead (Fig. 6(i,j)). Furthermore, the single bead became asymmetric with the emergence of apparent spatters when d_2 reached 4 mm (Fig. 6(k,1)). Additionally, when d_2 further increased to 5 mm (Fig. 6(m)), the amount of the spatter in the single layer increased significantly, and large porosity also occurred, which was mainly attributed to the significant instability and strong oscillation of the molten pool owing to the excessive d_2.

3.4. Multi-layer single-bead additive manufacturing

The final ten-layer thin-walled parts deposited by TTWIA are shown in Fig. 7. Generally speaking, the part was deposited successively without the overflowing and collapsing of the molten pool. In this section, the surface roughness [18] and material utilization rate [32] of the component were introduced aimed to quantitatively characterize the geometric accuracy of the parts. When the wire-tungsten distance (d_1) and tungsten-tungsten distance (d_2) were both 2 mm (Fig. 7(a-c)), the forming surface became smooth, and the adjacent-layer boundary was clear, with a roughly consistent overall height. In detail, the surface roughness and material utilization rate of the deposited part were 1.21 mm and 83.74% respectively. An irregular cross section and the worse forming surface with mixed-twisted layers and large protrusions were observed when d_1 increased to 3 mm (Fig. 7(d-f)). The appearance of the protrusion resulted from the solidification of the overflow of the molten pool. Specifically, the surface roughness of the formed part increased to 1.47 mm , while the material utilization rate decreased to 77.07%. It indicated that the increase of d_1 reduced the shape accuracy of the part deposited by TTWIA additive manufacturing. Additionally, when d_1 further increased to 4 mm (Fig. 7(g,h)), obvious pores and collapse were generated in the thin-walled part. This was mainly attributed to the inadequate protective effect and unstable molten pool on account of the excessive d_1.

Similarly, when d_2 increased to 3 mm (Fig. 7(i-k)), the side surface quality decreased evidently with apparent protrusions, even if no pore, inclusion, or lack of fusion appeared on the cross section of the thin-walled part. Specifically, the surface roughness of the formed part increased to 1.84 mm , while the material utilization rate decreased to 74.72%. Besides, when d_2 further increased to 4 mm (Fig. 7(1,m)), the tumor-like protrusions increased, and the pores appeared in the thin-walled part. This phenomenon was closely associated with the poor protection on the molten pool caused by the excessive d_2.

WAAM process was carried out through the transfer of the high-temperature liquid metal droplets. As the number of the deposited layers increased, the heat accumulation in the component increased, making it difficult for the molten pool to solidify and complicating the control of the deposited layer's shape. Fig. 8 shows the driving forces acting on molten pool in TTWIA deposition process. According to previous analysis, these forces primarily contained arc pressure F_P, droplet impingement force F_D, arc shear force F_τ, gravity F_G, Marangoni force F_M, and normal reaction F_N, and each of them served a different function [24, 33].

As d_1 or d_2 increased, the lateral flow tendency in the molten pool was weakened due to the lower F_P and F_D, caused by the decreased arc current density, which led to the larger wetting angle and smaller width of the deposited layer. Consequently, F_N in the current layer was relatively

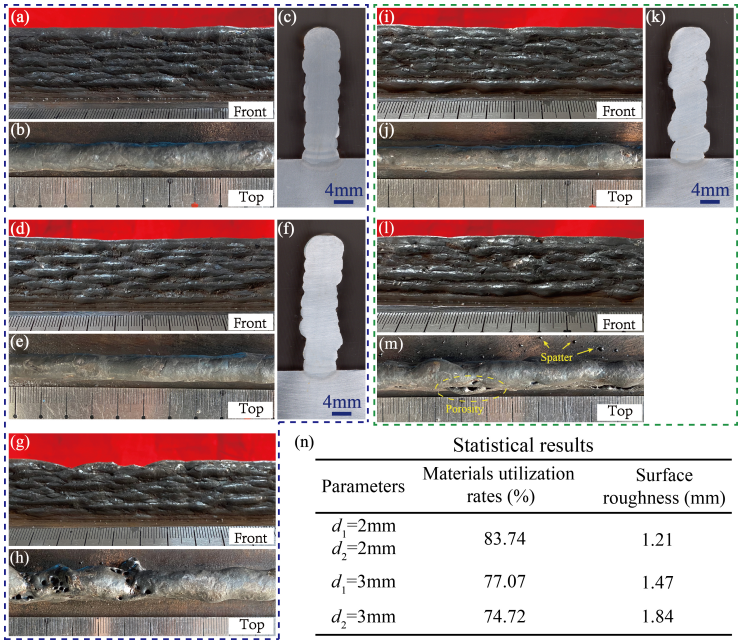

(n) Statistical results

Parameters	Materials utilization rates (%)	Surface roughness (mm)
d_1=2mm d_2=2mm	83.74	1.21
d_1=3mm	77.07	1.47
d_2=3mm	74.72	1.84

Fig. 7. Surface morphology and cross sections of deposited parts of TTWIA multi-layer single-pass. (a,b,c) $d_1 = 2$ mm, $d_2 = 2$ mm; (d,e,f) $d_1 = 3$ mm; (g,h) $d_1 = 4$ mm; (i,j,k) $d_2 = 3$ mm; (l,m) $d_2 = 4$ mm; (n) Deposited part parameters.

lower, which contributed to the process instability, and thus the molten pool inevitably flowed down from the component. Therefore, the surface finish and dimensional accuracy of the deposited part were both deteriorated to some extent.

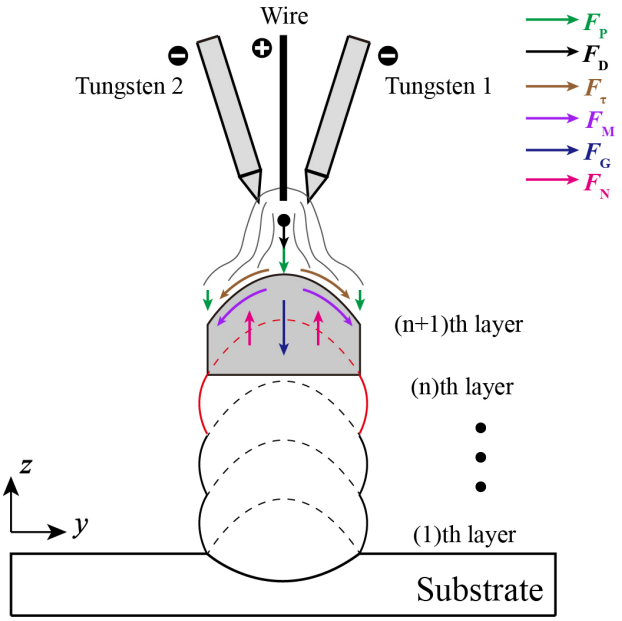

Fig. 8. Schematic diagram of TTWIA deposition forming and force analysis.

4. Conclusions

In this paper, the influences of wire-tungsten (d_1) and tungsten-tungsten (d_2) spacing on the forming characteristic of TTWIA additive manufacturing were separately studied. The following conclusions were drawn.

1. As d_1 or d_2 increased, the arc shape of TTWIA diverged and the coupling intensity was weakened, because of the lower current density and smaller self-induced magnetic field strength caused by the elongated conductive channel of the arc. Besides, the liquid stream became thick as well as the larger droplet diameter and lower transfer frequency owing to the increased surface tension and decreased electromagnetic force and arc pressure acting on the droplet.

2. The transverse flow tendency of liquid metal was diminished, and the molten pool width of TTWIA decreased with the increase of d_1 or d_2, which caused that the height/width ratio and the wetting angle of the deposited bead increased. This was mainly because of the decreased arc pressure, droplet impingement force and Marangoni force, resulted from the declined arc current and reduced droplet transfer frequency.

3. The surface quality and geometric accuracy of the thin-walled part fabricated by TTWIA deteriorated as d_1 or d_2 increased, with the increased surface roughness and reduced material utilization rate, which mainly

resulted from the instability of the molten pool because of the lowered normal reaction acting on the present deposited layer, caused by the growing wetting angle and reduced width of the deposited layer.

Acknowledgements

This work was supported by Shandong Provincial Natural Science Foundation (ZR2024QE323), and Key R&D Program of Shandong Province, China (Initiative for Enhancing the Innovation Capability of Technology-based SMEs) (2025TSGCCZZB0408).

References

[1] Z. Chen, L. Yuan, Z. Pan, H. Zhu, N. Ma, D. Ding, and H. Li, (2025) *"A comprehensive review and future perspectives of simulation approaches in wire arc additive manufacturing (WAAM)"* **International Journal of Extreme Manufacturing 7**: 022016. DOI: 10.1088/2631-7990/ada099.

[2] M. Dekis, M. Tawfik, M. Egiza, and M. Dewidar, (2025) *"Challenges and developments in wire arc additive manufacturing of steel: A review"* **Results in Engineering *26***: 104657. DOI: 10.1016/j.rineng.2025.104657.

[3] S. Gain and D. Veeman, (2025) *"A review on advances and challenges in wire arc additive manufacturing: Process parameters, microstructural evolution and material performance across alloys"* **Journal of Alloys and Compounds *1029***: 180735. DOI: https://doi.org/10.1016/j.jallcom.2025.180735.

[4] J. Norrish, J. Polden, and I. Richardson, (2021) *"A review of wire arc additive manufacturing: development, principles, process physics, implementation and current status"* **Journal of Physics D: Applied Physics *54***: 473001. DOI: 10.1088/1361-6463/ac1e4a.

[5] S. Huang, X. Zeng, X. Du, Z. Peng, J. Li, R. Wang, J. Liu, B. Yan, J. Liu, Z. Cai, H. Wang, and C. Liu, (2023) *"Microstructure and mechanical properties of the Nb37.7Mo14.5Ta12.6Ni28.16Cr7.04 multi-principal alloys fabricated by gas tungsten wire arc welding additive manufacturing"* **Vacuum *210***: 111900. DOI: https://doi.org/10.1016/j.vacuum.2023.111900.

[6] Y. Ke and J. Xiong, (2020) *"Microstructure and mechanical properties of double-wire feed GTA additive manufactured 308L stainless steel"* **Rapid Prototyping Journal *26***: 1503–1513. DOI: 10.1108/RPJ-09-2019-0238.

[7] P. Schilling, T. Ungethum, P. Sanderbrand, and H. C. Schmale, (2026) *"Investigation of a multi-cathode TIG arc process for additive manufacturing applications"* **Welding in the World *64***: 1329–1340. DOI: 10.1007/s40194-026-02414-1.

[8] S. X. Lv, X. B. Tian, H. T. Wang, and S. Q. Yang, (2007) *"Arc heating hot wire assisted arc welding technique for low resistance welding wire"* **Science and Technology of Welding and Joining *12***: 431–435. DOI: 10.1179/174329307X213828.

[9] A. L. Voigt, T. V. d. Cunha, and C. E. Niño, (2020) *"Conception, implementation and evaluation of induction wire heating system applied to hot wire GTAW (IHW-GTAW)"* **Journal of Materials Processing Technology *281***: 116615. DOI: https://doi.org/10.1016/j.jmatprotec.2020.116615.

[10] Q. Han, X. Li, M. Dong, and G. Zhang, (2021) *"Enhanced curve-fitting model of the bead section profile and the corresponding overlapping model for twin-electrode gas tungsten arc-based additive manufacturing"* **International Journal of Advanced Manufacturing Technology *116***: 1151–1167. DOI: 10.1007/s00170-021-07501-9.

[11] S.-C. Park, H.-S. Bang, and W.-J. Seong, (2020) *"Effects of material properties on angular distortion in wire arc additive manufacturing: experimental and computational analyses"* **Materials *13***: 1399. DOI: 10.3390/ma13061399.

[12] T. Zhang, L. Wang, C. Xu, J. Cheng, and K. Wang, (2023) *"Early-warning system for copper alloy abnormal molten pool in wire-arc additive manufacturing via convolutional neural network method"* **Journal of Materials Engineering and Performance *32***: 11230–11239. DOI: 10.1007/s11665-023-07949-8.

[13] X. Zhang, F. Martina, J. Ding, X. Wang, and S. W. Williams, (2017) *"Fracture toughness and fatigue crack growth rate properties in wire + arc additive manufactured Ti-6Al-4V"* **Fatigue & Fracture of Engineering Materials & Structures *40***: 790–803. DOI: 10.1111/ffe.12547.

[14] T. Hauser, R. T. Reisch, P. P. Breese, B. S. Lutz, M. Pantano, Y. Nalam, K. Bela, T. Kamps, J. Volpp, and A. F. H. Kaplan, (2021) *"Porosity in wire arc additive manufacturing of aluminium alloys"* **Additive Manufacturing *41***: 101993. DOI: 10.1016/j.addma.2021.101993.

[15] F. Wang, S. Williams, and M. Rush, (2011) *"Morphology investigation on direct current pulsed gas tungsten arc welded additive layer manufactured Ti6Al4V alloy"* **International Journal of Advanced Manufacturing Technology *57***: 597–603. DOI: 10.1007/s00170-011-3299-1.

[16] S. Teng, S. Dehgahi, H. Henein, T. Wolfe, and A. J. Qureshi, (2025) *"Sensor-fusion enabled inter-layer temperature control of nano-treated 7075 aluminum alloy produced through wire-arc directed energy deposition process"* **Progress in Additive Manufacturing *10***: 1293–1314. DOI: 10.1007/s40964-024-00707-9.

[17] J. A. Tröger, S. Hartmann, K. Treutler, A. Potschka, and V. Wesling, (2025) *"Simulation-based process parameter optimization for wire arc additive manufacturing"* **Progress in Additive Manufacturing *10***: 1–14. DOI: 10.1007/s40964-024-00597-x.

[18] J. Long, M. Wang, W. Zhao, X. Zhang, Y. Wei, and W. Ou, (2022) *"High-power wire arc additive manufacturing of stainless steel with active heat management"* **Science and Technology of Welding and Joining *27***: 256–264. DOI: 10.1080/13621718.2022.2045127.

[19] C. Ma, C. Li, Y. Yan, Y. Liu, X. Wu, D. Li, Y. Han, H. Jin, and F. Zhang, (2021) *"Investigation of the in-situ gas cooling of carbon steel during wire and arc additive manufacturing"* **Journal of Manufacturing Processes *67***: 461–477. DOI: 10.1016/j.jmapro.2021.05.022.

[20] J. Liu, Y. Miao, Z. Wang, Y. Zhao, Y. Wu, and C. Li, (2024) *"Improved strength in nickel-aluminum bronze/steel bimetallic component fabricated using arcing-wire arc additive manufacturing with alternating deposition strategy"* **Journal of Manufacturing Processes *111***: 89–103. DOI: 10.1016/j.jmapro.2024.01.027.

[21] S. Chen, S. Zhang, N. Huang, P. Zhang, and J. Han, (2016) *"Droplet transfer in arcing-wire GTAW"* **Journal of Manufacturing Processes *23***: 149–156. DOI: 10.1016/j.jmapro.2016.05.014.

[22] J. Wang, D. Wu, P. Liao, C. Y. Tian, M. Q. Li, and J. C. Feng, (2013) *"Metal transfer and arc behaviour of novel consumable and non-consumable electrode indirect arc droplet welding"* **Science and Technology of Welding and Joining *18***: 261–270. DOI: 10.1179/1362171812Y.0000000103.

[23] Y. Zhu, Z. Wang, R. Liu, and L. Liu, (2022) *"Study on arc behavior and droplet transfer in twin-electrode TIG-MIG indirect arc welding"* **International Journal of Advanced Manufacturing Technology *120***: 6821–6831. DOI: 10.1007/s00170-022-09131-1.

[24] Y. Zhu, R. Liu, and L. Liu, (2023) *"A comparison of single and twin tungsten electrode - wire electrode IAW"* **Materials and Manufacturing Processes *38***: 1436–1444. DOI: 10.1080/10426914.2022.2146715.

[25] L. Liu, Y. Zhu, and R. Liu, (2023) *"Study of twin tungsten electrode-wire electrode indirect arc welding assisted by alternating magnetic field"* **Journal of Manufacturing Processes *101***: 171–180. DOI: 10.1016/j.jmapro.2023.06.007.

[26] Y. Zhu, S. Gao, S. Yu, and D. Ma, (2025) *"Forming characteristic analysis in twin tungsten electrode - Wire electrode indirect arc based additive manufacturing"* **Vacuum *232***: 113902. DOI: 10.1016/j.vacuum.2024.113902.

[27] L. Liu, S. Yu, G. Song, and C. Hu, (2019) *"Analysis of arc stability and bead forming with high-speed TW-GIA welding"* **Journal of Manufacturing Processes *46***: 67–76. DOI: 10.1016/j.jmapro.2019.08.023.

[28] Y. Wu, Z. Li, X. Wang, Y. Feng, M. Wang, and J. Shan, (2022) *"Narrow groove laser-arc hybrid welding of thick-sectioned HSLA steel using laser beam oscillation"* **Welding Journal *101***: 181S–196S. DOI: 10.29391/2022.101.014.

[29] K. Li, C. Jia, C. Fang, J. Hu, S. Xu, Y. Wang, and C. Wu, (2024) *"Numerical simulation of the unique rotating arc behaviors during narrow-groove GTAW"* **Journal of Manufacturing Processes *131***: 1611–1623. DOI: 10.1016/j.jmapro.2024.09.109.

[30] R. Zong, J. Chen, C. S. Wu, and G. K. Padhy, (2017) *"Influence of molten metal flow on undercutting formation in GMAW"* **Science and Technology of Welding and Joining *22***: 198–207. DOI: 10.1080/13621718.2016.1214406.

[31] K. C. Mills, B. J. Keene, R. F. Brooks, and A. Shirali, (1998) *"Marangoni effects in welding"* **Philosophical Transactions of the Royal Society A: Mathematical, Physical and Engineering Sciences *356***: 911–925. DOI: 10.1098/rsta.1998.0196.

[32] C. Ma, Y. Yan, Z. Yan, Y. Liu, X. Wu, D. Li, M. Zhang, P. Liu, and H. Jin, (2023) *"Efficient manufacturing of Al-Mg alloys using controlled low heat input wire and arc additive manufacturing"* **Journal of Materials Processing Technology *314***: 117899. DOI: 10.1016/j.jmatprotec.2023.117899.

[33] Y. Li, R. Zong, Y. Zhang, and B. Zhang, (2024) *"Numerical simulation of molten pool behavior and bead formation in Al-alloy GMAW bead-on-plate welding"* **Welding in the World *68***: 2293–2309. DOI: 10.1007/s40194-024-01754-0.